JOURNAL OF MATERIALS SCIENCE 11 (1976) 1339–1346

Investigation of short range ordering in polymers by means of radial distribution functions derived from X-ray diffraction

Part 2 *Polyethylene terephthalate*

G. W. LONGMAN
Imperial Chemical Industries Limited, Corporate Laboratory, Runcorn, Cheshire, UK

R. P. SHELDON
School of Polymer Science, University of Bradford, Bradford, UK

G. D. WIGNALL
Imperial Chemical Industries Limited, Europa Division, Everslaan 45, B3078 Everberg, Belgium

Four samples of polyethylene terephthalate (PET), with different thermal histories were investigated by radial distribution function (RDF) methods. Intramolecular distances in the polymer repeat unit were successfully attributed to peaks in the RDF plot up to values of $r \sim 5$ Å. A broad peak at ~ 4 Å was attributed to nearest neighbour intermolecular ordering, but there was no evidence of ordering beyond this distance in samples annealed for prolonged periods at temperatures close to the polymer T_g. This evidence does not support previous models proposing the presence of extensive para-crystalline ordering in amorphous PET. Low frequency broad peaks, with a periodicity of ~ 4 Å, were resolved out to values of $r \sim 20$ Å in the RDF plot for a sample with a density crystallinity index of $\sim 20\%$, thus confirming the sensitivity of the RDF analysis to short range intermolecular ordering.

1. Introduction

Amorphous polymers have long been considered to be structureless arrangements of macromolecules, possessing only short range liquid like order. The presence of interchain entanglements and free volume have been invoked to explain many of the observed physical properties of these polymers. This state has been conveniently described by Flory's random coil model [1]. A number of recent studies have suggested that amorphous polymers possess structure on a scale greater than the dimensions of the polymer repeat unit. In particular Geil and co-workers have suggested that a paracrystalline ordering, characterized by ball like structures, is present in amorphous polycarbonate [2] and polyethylene terephthalate (PET) [3]. These balls have been observed by electron microscopy, on the free surface of bulk material and in thin solution cast films, and are postulated to move and align at temperatures close to the glass–rubber transition temperature (T_g) of the polymer. Extensive annealing is claimed to result in structures suggesting the initial growth stages of spherulites. This concept of structure may be assumed to require an appreciable level of ordering in the sample. It has been suggested that amorphous polymers contain ordered domains or bundles within which the molecular segments are aligned over large distances compared to the size of the repeat unit [4, 5]. The chain packing is such that the segments lie approximately parallel and equidistant to each other. Thermal analysis evidence relating to endothermal peaks observed near the T_g has

also been cited in support of the concept of ordering in amorphous polymers [6]. Ali and Sheldon [7] have reported similar endothermal peaks in PET immediately above the transition region by differential thermal analysis (DTA) and differential scanning calorimetry (DSC).

Other workers [8] have suggested that although there is some evidence of ordering in amorphous PET samples after annealing at temperatures just above T_g, there is no evidence of similar structures occurring as a result of annealing below T_g. Moreover, endothermal peaks observed in samples thus treated may be accounted for by overheating phenomena arising from enthalpy effects related to changes in free volume [9]. Whatever the interpretation placed upon these endothermal peaks, the samples are still "amorphous" when judged by the widely used criterion that the material does not give an X-ray diffraction pattern comprising sharp Bragg reflections. Ali and Sheldon [10] used a wide range of techniques including small-angle X-ray scattering, infra-red and laser-Raman in an attempt to distinguish between the various interpretations. They concluded that within the sensitivity of the techniques there was no evidence to support the concept of local ordering of chains.

The short range order in "amorphous" materials can be characterized by means of radial distribution function (RDF) method [11], derived from an analysis of the scattered diffraction pattern from the material. Previous work [12, 13] has shown that RDF methods can resolve both intramolecular and intermolecular ordering in polymers. These techniques have been applied to four samples of polyethylene terephthalate in an attempt to determine whether there is any substantial long range ordering, in addition to the short range liquid like order, generally assumed to be present. In preparing samples we have attempted to duplicate the annealing conditions under which structural features have been reported by electron microscopy [3].

2. Theory and data collection

The rigorous theory of scattering from a system containing more than one kind of atom has been given by Waser and Schomaker [11] and Pings and Waser [14]. The intensity of radiation scattering coherently from a sample is measured as a function of scatter angle 2θ, over as wide an angular range as possible in the experiment. The scattering variable is conventionally converted from 2θ to $s = 4\pi/\lambda \sin\theta$ where λ is the wavelength of the incident and (elastically) scattered radiation. The intensity is corrected for experimental conditions and normalized to electron units. Then the Fourier transform gives to a good approximation an average of the different atomic correlation functions, weighted by the atomic concentrations of the atoms and their scattering factors [13].

The details of the experimental procedures for data collection and analysis are similar to those used for studies of bisphenol-A polycarbonate [13]. Diffraction data were collected on a Picker automatic four circle diffractometer aligned in the transmission geometry and employing a molybdenum target ($K\alpha$ wavelength = 0.7107 Å) with balanced Zr–Yt Ross filters on the incident beam to monochromatize the incident radiation. The collimation divergence limits were chosen by reducing the limits until no detectable change in the shape of the diffraction pattern was observed.

For most of the data collection these were set at 0.5°, so that when the detector was positioned at an angle 2θ, the measured intensity has been scattered between $2\theta \pm \frac{1}{2}°$. The divergence angles were halved by using smaller collimators to measure accurately at low angles near the main beam. The low angle scan was subsequently normalized to the main data scan in the angular range $\theta = 8°$ to 15°.

Intensities were measured over the range $\theta = 0.5°$ to 66.0° at angular intervals of $\theta = 0.075°$ upto $\theta = 15°$, and intervals of 0.25° thereafter upto $\theta = 66°$, giving a range of $s = 4\pi/\lambda \sin\theta$ of 0.15 to 16.15 $Å^{-1}$. Data were collected on a fixed count basis, i.e. the time for a fixed count (10 000) on each of the two filters was recorded and subsequently converted to a plot of count rate of a given time interval.

Four samples of polyethylene terephthalate were examined, in the form of flat sheets approximately 25 mm square and 0.6 mm thick. Sample A was quenched from the melt to room temperature on a cold roll, and sample B, C and D were subsequently annealed for 100 h at 65, 80 and 90° C respectively. The measured densities were 1.337, 1.336 and 1.359 for samples A, C and D respectively.

Figs. 1 and 2 show smoothed plots of $I_{sm}(\theta) = I^{\beta} - I^{\alpha}$ corrected for incident intensity drift by repeated checks on the intensity of a fixed angle at regular intervals throughout the run (intensity of a fixed angle at regular intervals throughout the run (intensity drifts are small, ~ 2%). Fig. 1 shows a

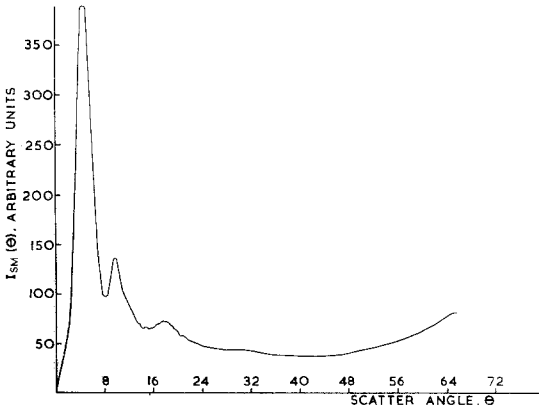

Figure 1 I_{sm} (θ) versus θ for sample A.

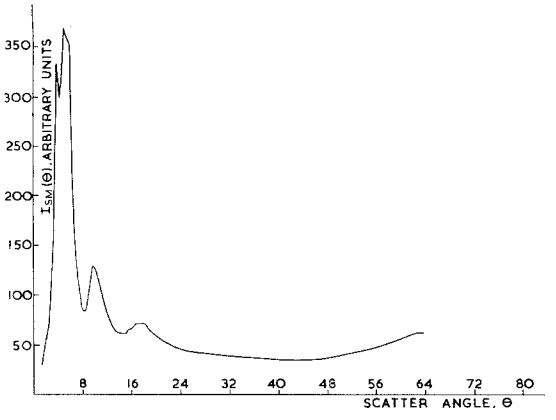

Figure 2 $I_{sm}(\theta)$ versus θ for sample D.

plot typical of samples A, B and C, whilst Fig. 2 shows the plot for sample D which was annealed at the highest temperature (90° C).

3. Data analysis

The experimentally measured intensity curve was corrected for absorption of the incident and diffracted beams in the sample. The background scattering was measured for both the main scans and low-angle scans in the absence of a sample, and corrected for absorption by the sample before subtraction from the intensity data. This background was less than 2% of the sample scattering over most of the angular range.

The problem of removing that component of the scattered radiation which has undergone multiple scattering has been discussed by Wignall *et al.* [15], and first order corrections for double scattering factors of Berghius [16] and Stewart described in [13]. The arbitrary units of the intensity measurements were also corrected for polarization effects, and normalized to electron units using the dispersion corrected coherent scattering factors of Berghius [16] and Steward [17] and incoherent scattering factors of Keating and Vineyard [18], Sagel [19] and Freeman [20]. The effect of different methods of normalization [21] on the value of transformed RDF curve at very low values of r is discussed in detail elsewhere [22].

The RDF, $H(r)$, is defined by

$$H(r) = \frac{1}{2\pi^2 \bar{p} r} \int_0^\infty si(s) \sin sr ds$$

where $\bar{p}$ is the mean atomic density for one system the scattering data (see [13]). Experimental RDF's were generated by an IBM Fourier transform routine.

$H(r)$ as defined by the above equation requires values of $si(s)$ from 0 to infinity, but in practice values are available only in the range $s = \sim 0.15$ to $\sim 16\,\text{Å}^{-1}$. The truncation of $si(s)$ at s_{max} may introduce spurious high frequency oscillations in the RDF with a frequency $2\pi/s_{max}$. The causes and appearance of truncation errors are discussed in some detail by Voigt-Martin and Mijlhoff [23] for RDF curve obtained by electron diffraction. Electron diffraction offers the facility to collect data at greater values of s_{max} (up to $30\,\text{Å}^{-1}$) than used in the present work, and thus reduce the effects of high frequency termination ripples. Conversely, X-ray diffraction allows data to be obtained at lower values of s_{min}, thus enabling meaningful information to be obtained for larger values of r. A comparison of recent determinations of $H(r)$ in molten polyethylene by electron diffraction with $s_{max} = 25\,\text{Å}^{-1}$ [23] and by X-ray diffraction using the present system [24] shows a large measure of agreement in the positions and intensities of the peaks resolved. This indicates that the peaks resolved represent real structural features, rather than truncation artefacts, in view of the wide differences in truncation limits employed. This conclusion is reinforced by a comparison of the experimental peak positions with those expected from short range intramolecular distances [23]. The observed peaks up to 5 Å are all predicted by the short range intramolecular ordering determined by the possible chain configurations. A similar conclusion has been reached in the cases of RDF studies of vitreous carbon [25] and bisphenol-A polycarbonate [13], and shows that truncation errors are not a serious artefact in $H(r)$ with the present

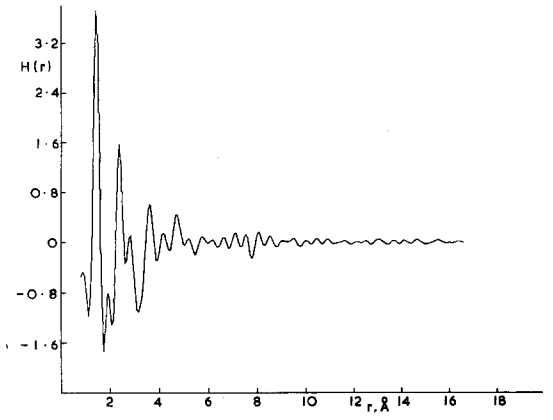

Figure 3 $H(r)$ versus r for sample A

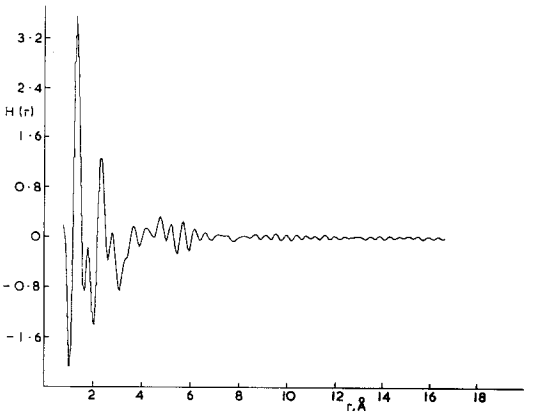

Figure 4 $H(r)$ versus r for sample B.

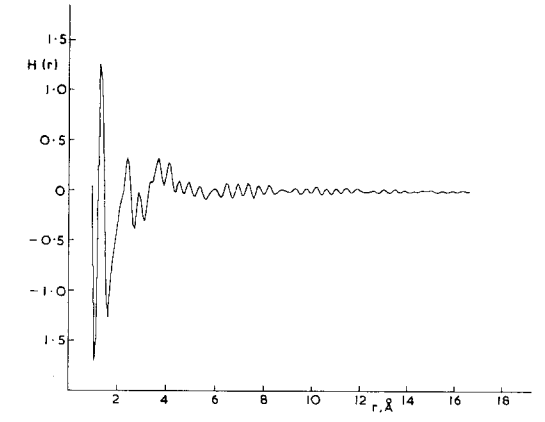

Figure 5 $H(r)$ versus r for sample C.

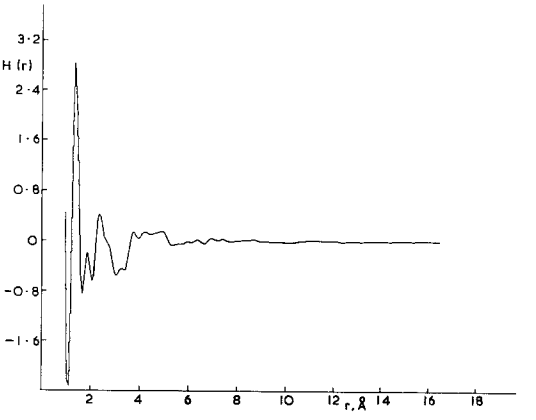

Figure 6 $H(r)$ versus r for sample D.

diffraction system. A comparison of the observed peaks in $H(r)$ for polyethylene terephthalate with those expected from the known intramolecular order is given in Section 4. It will be seen that there are no spurious features below $r = 5$ Å, the peaks being attributable to intramolecular distances, and hence no damping factor [26], has been applied to $si(s)$ before transformation. "Undamped" plots of $H(r)$ are shown in Figs. 3, 4, 5 and 6 for samples A, B, C and D respectively.

However, for $r > 5$ Å in view of the increasing number of similar interatomic distances, one would not expect sharp maxima in the RDF. Thus the small oscillations between 7 and 16 Å probably represent residual truncation errors, as their frequency is approximately given by $2\pi/S_{max} \approx 0{\cdot}4$ Å, as expected for truncation features [26]. These features are small in $H(r)$, but when examining the RDF for intermolecular ordering over an extended range of r space, it is best to plot the second moment of $H(r)$. The small truncation oscillations are then considerably magnified by the r^2 factor, and hence such plots have been damped by multiplying $i(s)$ by an exponential factor $e^{-\alpha^2 S^2}$ before transformation.

4. Discussion

Polyethylene terephthalate crystallizes readily over a wide range of temperatures [27] but may also be obtained in the amorphous state by quenching rapidly from the melt to below the glass-rubber transition temperature. The observation by Yeh and Geil [3] of ball-like structures in amorphous PET, and the attribution of paracrystalline order to these structures has produced considerable interest in the structure of amorphous polymers.

In general the peaks observed in the RDF plot for a polymer should be attributable either to

intramolecular atomic distances arising from the polymer repeat units, or to intermolecular atomic distances determined by the short range ordering or packing of the polymer chains. Earlier work has shown that both intramolecular and intermolecular distances may be satisfactorily resolved in samples of polystyrene [12] and bisphenol-A polycarbonate [13]. A similar approach has been adopted for PET in this work. Fig. 7 shows the

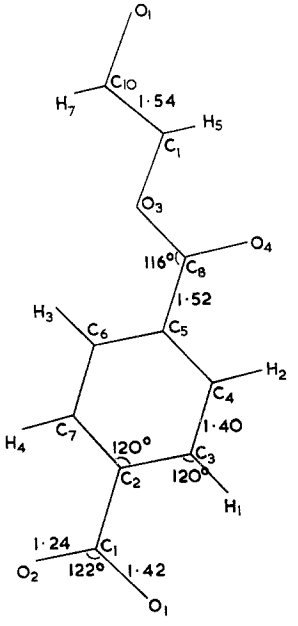

Figure 7 Assumed bond lengths and bond angles for the PET repeat unit.

assumed molecular conformation for the polymer repeat unit. This is essentially the conformation of the unit in the crystal unit cell [28] with the simplifying assumptions that the carbonyl groups are planar with the benzene ring, and that the methyl groups are in the planar zig-zag configuration.

In view of the fact that the phenyl ring and adjacent carboxyl groups form a relatively rigid segment, it is not unreasonable to use this conformation for calculating the expected intramolecular distances, at least up to distances ~5 Å. Above this distance, the conformation becomes increasingly uncertain in view of the ability of the chain to rotate about C–C bonds or O–CH2 bonds in the glycol segment. Hence, comparison of expected intramolecular distances with the peaks found in the RDF has been limited to distances less than 5 Å.

The intensity or area under the RDF peak resulting from an i–j bond at r_{ij} has been defined by Mozzi and Warren [26] as

$$A_{ij} = \sum_{uc}\sum_{i}\frac{N_{ij}}{r_{ij}} z_i z_j \frac{\pi}{2}$$

where z_i and z_j are the atomic number of ith and jth atoms, r_{ij} is the distance between these atoms, N_{ij} is the number of neighbours in the jth shell about the i atom and $\sum_{uc}$ refers to a summation over a unit of composition, which is the polymer repeat unit.

The interatomic distances calculated for the assumed conformation, together with the values of A_{ij} and the observed RDF peak distances are listed in Table I. The interatomic distances fall into seven groups, whose average position matches reasonably well with the seven observed peaks in the RDF. The biggest discrepancy involves the peak at ~2·0 Å, where the interatomic distances are ~14% higher than the observed RDF peak. However, as this peak originates from atom pairs involving hydrogen atoms, some of the discrepancy may be attributed to the shift of electron density into the bond, as discussed for the case of bisphenol-A polycarbonate [13] where similar discrepancies were observed. The other groups fall within a few percent of the observed RDF peak distances.

Intermolecular ordering is best observed by plotting $4\pi r^2 \bar{\rho} H(r)$ over an extended range of r space, having applied a damping factor $\alpha = 0.17$ to the data. This value was chosen to eliminate most of the high frequency (0.4 Å) truncation oscillation, while leaving the lower frequency (5 Å) structural features unaffected. Figs. 8 to 11 show plots of $4\pi r^2 \bar{\rho} H(r)$ versus r for samples A to D respectively. In samples A, B and C a single broad peak is just resolvable in the region $r \approx 5$ Å,

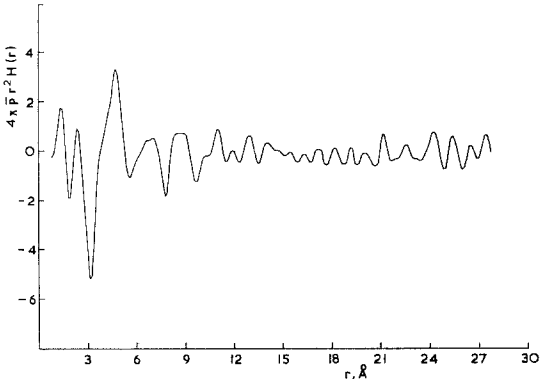

Figure 8 $4\pi r^2 \bar{\rho} H(r)$ versus r for sample A.

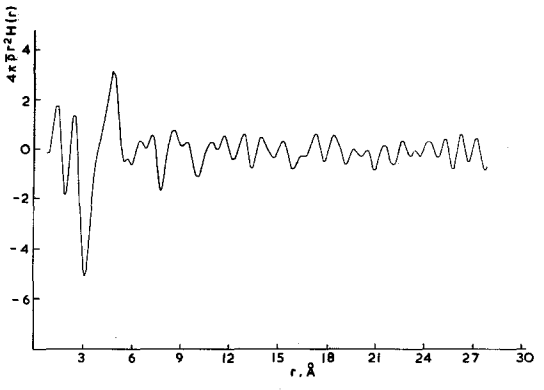

Figure 9 $4\pi r^2\bar{\rho}H(r)$ versus r for sample B.

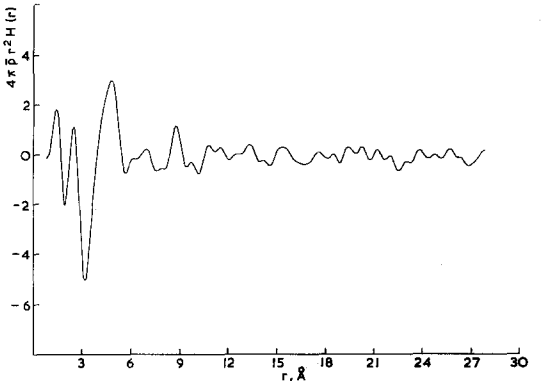

Figure 10 $4\pi r^2\bar{\rho}H(r)$ versus r for sample C.

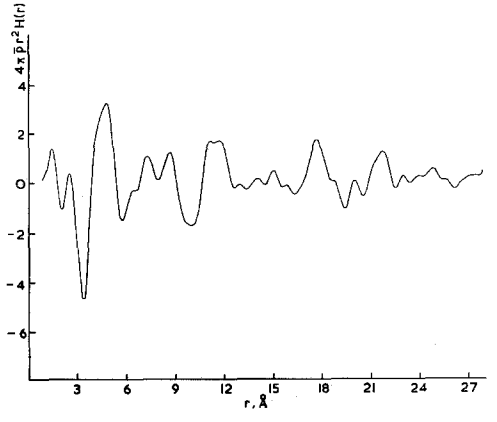

Figure 11 $4\pi r^2\bar{\rho}H(r)$ versus r for sample D.

upon which the peaks attributed to intramolecular distances are superimposed. This may be interpreted as the nearest neighbour chain interaction determined by the physical size of the polymer chains; no interchain ordering is resolvable at greater distances, i.e. larger values of r. Fig. 12 shows the plot for the more highly ordered sample D which has a "crystallinity" of approximately 20% determined by its density. This shows well resolved peaks at r ~4.5, 11, 17.5, 21.5 Å which reflect the intermolecular short range ordering in the sample. The correlation apparently extends over distances of 20 Å but is not observed at greater distances. It is not necessary to postulate ordering beyond approximately 10 Å in samples A, B and C to be consistent with the observed RDF plots. The available evidence does not indicate that ordering has increased in the sample annealed at either 65 or 80° C, and thus does not appear to be consistent with previous models [4, 5] proposing appreciable levels of interchain ordering in the amorphous state. The resolution of interchain ordering in sample D indicates that the RDF technique would have resolved substantial interchain ordering in samples A, B and C had it been present at the level postulated. As stated in the introduction, the thermo-analytical data [6, 7, 9] has been the subject of more than one interpretation, and has been used as evidence for [6] and against [9] substantial interchain ordering. The RDF data reveal little interchain ordering after annealing near T_g and thus appears to support the interpretation of Petrie [9]. The data of Ali and Sheldon [10] show that even if the endothermic maxima are taken as evidence of ordering, the maximum degree of order which may be produced by annealing PET near T_g is equivalent to a density crystallinity index of approximately 1%. Such a low level of order is consistent with the RDF data and an overall morphology possessing little interchain ordering. It is worth noting that generally for both the amorphous and annealed samples the diffraction pattern revealed only smooth broad peaks, with no suggestions of sharp discrete Bragg reflections. The exception to this is sample D which was annealed at 90° C. The resultant increased ordering in the sample is reflected by the increase in density to 1.359, equivalent to a crystallinity index of ~20%, and by the additional line in the diffraction pattern (see Fig. 2). No change in the diffraction pattern is observed in the samples annealed at 65 and 80° C compared to the unannealed material. our findings are similar in this respect to those of Kilian *et al.* [29]. Yeh and Geil noted that after prolonged annealing of thin films at similar temperatures near T_g, (1 1 1) and (0 1 1) Bragg reflections appeared in addition to the broad amorphous

TABLE I

	Interatomic distance	r_{ij}	A_{ij}	RDF peak
C–O	Carbonyl double bond, C_1–O_2 etc	1.24	243.2	1.43
C–O	Carbonyl single bond, C_1–O_1 etc	1.42	424.7	
C–C	Aromatic C–C in ring C_2–C_3 etc	1.40	484.7	
C–C	Aliphatic C–C ethylene sequence, C_9–C_{10} etc	1.54	220.3	
H–H	Inter hydrogen distance on methyl groups	1.77	3.5	
O–H	O– to H in 1st methyl, O_3–H_5 etc	2.14	23.4	1.92
C–H	Aliphatic carbon to H in other methyl, C_{10}–H_5 etc	2.15	17.5	
C–H	Hydrogen to next C in ring H_1–C_2 etc	2.2	68.5	
O–H	Carboxyl O– to H in methyl, O_4–H_5 etc	2.24	33.6	
O–O	Inter oxygen distance carboxyl group, O_1–O_2 etc	2.33	86.3	2.40
C–C	Next but one C in ring, C_2–C_4 etc	2.42	280.4	
H–H	Inter hydrogen dist. in ring, H_1–H_2 etc	2.44	2.6	
C–C	Carboxyl C to methyl C, C_8–C_9 etc	2.48	91.2	
O–H	Carboxyl O to H in ring, O_1–H_1 etc	2.49	20.2	
C–O	1st ring carbon to carboxyl O, C_2–O_2, C_5–O_4 etc	2.51	120.1	
C–C	Aliphatic C to next but one in ring, C_1–C_3 etc	2.54	133.5	
C–O	Carboxyl O to 1st ring carbon, C_2–O_1	2.61	115.4	
O–H	Carboxyl O to H in ring, O_2–H_4 etc	2.61	19.2	
C–O	Carboxyl O to C in methyl, O_4–C_9 etc	2.61	115.5	
O–H	Carboxyl O to H in second methyl, O_3–H_7 etc	2.71	37.1	2.86
C–H	Carboxyl C to H in first methyl C_8–H_5 etc	2.75	27.4	
C–C	Inter carbon distance across ring, C_2–C_5 etc	2.80	121.1	
O–C	Carboxyl O– second C in ring, O_1–C_3 etc	2.86	105.4	
O–C	Carboxyl O– second C in ring, O_2–C_7 etc	2.91	103.6	
C–H	H to next but two C in ring, H_2–C_2 etc	3.37	44.7	3.68
O–C	Carboxyl O– to 2nd C in ring, O_2–C_3 etc	3.67	82.1	
O–O	Carboxyl O– to carboxyl O–, O_1–O_3 etc	3.75	53.6	
O–C	Carboxyl O– to 2nd C in ring, O_1–C_7 etc	3.81	79.1	
C–H	Hydrogen to opposite C in ring, H_1–C_6 etc	3.89	25.8	
O–H	Carboxyl O–H in ring, O_2–H_1 etc	3.98	12.6	4.15
C–H	Carboxyl C to H in 2nd methyl, C_8–H_7 etc	4.1	18.3	
C–H	C in ring to H in 1st methyl, C_5–H_5	4.14	18.2	
O–H	Carboxyl O– to H in ring, O_1–H_4	4.15	12.1	
O–C	Carboxyl O– to 2nd methyl, O_4–C_{10} etc	4.22	71.4	
O–C	Carboxyl O– to 3rd ring carbon, O_1–C_4 etc	4.28	70.4	
O–C	Carboxyl O– to 3rd ring carbon, O_2–C_6 etc	4.31	69.9	
C–C	Carboxyl C to opposite ring carbon, C_2–C_8 etc	4.34	26.0	
C–C	Methyl C to 3rd ring carbon, C_9–C_6	4.41	51.3	
C–H	3rd carbon in ring to H in 1st methyl, C_6–H_5	4.82	15.6	4.77
O–C	Carboxyl O– to 3rd C in ring, O_2–C_4 etc	4.86	62.0	
O–C	Carboxyl C to O– across ethylene, C_1–O_3 etc	4.88	61.8	
O–H	Carboxyl O– to 2nd H in ring, O_1–H_2 etc	4.89	10.3	
O–H	Carboxyl O– to 2nd H in ring, O_2–H_3 etc	4.95	10.1	
O–C	Carboxyl O– to 3rd C in ring, O_3–C_3 etc	4.95	60.9	
O–O	Carboxyl O– to 0– across ethylene, O_2–O_3 etc	5.00	80.4	
C–C	Ring C to 2nd methyl C, C_5–C_{10} etc	5.00	45.2	

peaks. The X-ray measurements were made on bulk samples 0.6 mm thick, and this naturally raises the question of how closely the morphology of thin films (~1000 Å) mirrors that of the bulk. In view of the higher surface to volume ratio of the thin films, morphological changes on annealing do not necessarily parallel morphological changes in bulk samples. Thin film samples might, therefore, experience more intermolecular ordering on prolonged annealing near T_g.

The existence of only first neighbour packing is quite consistent with the ideas expressed in random coil model for amorphous polymers [1]. However, it is more difficult to explain on the

basis of the various bundle models which have been proposed for amorphous polymers, and which assume parallel packing of polymer chains over distances large compared to the repeat unit. One must assume at most second neighbour ordering of molecules in a plane perpendicular to the molecular axis. Also one must assume some kind of disordering along the chain, which randomizes the positions of the phenyl groups after 10 Å, otherwise intrachain correlations between strongly scattering groups (e.g. benzene rings) could be reflected by periodicities in the RDF. It is not necessary to assume correlations at distances greater than 10 Å to explain the RDF data for PET and it appears that the bundle models must at least be modified in the direction of greater randomness to accord with the data.

References

1. P. J. FLORY, *J. Chem. Phys.* **17** (1949) 303.
2. A. SIEGMANN and P. H. GEIL, *J. Macromol. Sci-Phys.* **B4** (1970) 239.
3. G. S. Y. YEH and P. H. GEIL, *ibid* **B1** (1967) 235.
4. R. E. ROBERTSON, *J. Phys. Chem.* **69** (1965) 1575
5. G. S. Y. YEH, *J. Macromol. Sci-Phys.* **B6** (1972) 465.
6. P. V. MCKINNEY and C. R. FOLTZ, *J. Appl. Polymer Sci.* **11** (1967) 1189.
7. M. S. ALI and R. P. SHELDON, *ibid* **14** (1970) 2619.
8. K. H. ILLERS, *Kolloid Z.* **245** (1971) 393.
9. S. E. PETRIE, *J. Polymer Sci.* **10** (1972) 1255.
10. M. S. ALI and R. P. SHELDON, *ibid* **C38** (1972) 97
11. J. WASER and V. SCHOMAKER, *Rev. Mod. Phys.* **48** (1968) 3016.
12. S. M. WECKER, T. DAVIDSON and J. B. COHEN, *J. Mater. Sci.* 7 (1972) 1249.
13. G. D. WIGNALL and G. W. LONGMAN, *ibid* 8 (1973) 1439.
14. C. J. PINGS and J. WASER, *J. Chem. Phys.* **48** (1968) 3016.
15. G. D. WIGNALL, J. A. J. JARVIS, W. E. MUNSIL and C. J. PINGS, *J. Appl. Cryst.* 7 (1974) 366.
16. J. BERGHUIS, I. J. BERTHA, M. HAANAPPEL, M. POTTERS, B. O. LOOPSTRA, V. H. MACGILLAVRY and A. L. VEENENDAAL, *Acta Cryst.* 8 (1955) 478.
17. R. F. STEWART, E. R. DAVIDSON and W. T. SIMPSON, *J. Chem. Phys.* **42** (1965) 3175.
18. D. T. KEATING and G. H. VINEYARD, *Acta. Cryst.* 9 (1956) 985.
19. K. SAGEL, "Tabellen zur Rontgenstrukturanalyse" (Springer-Verlag, Berlin, 1958).
20. A. J. FREEMAN, *Acta Cryst.* **12** (1959) 261.
21. J. KROGH-MOE, *ibid* **1** (1958) 267.
22. G. D. WIGNALL, R. N. ROTHON, G. W. LONGMAN, and G.R. WOODWARD, *J. Mater. Sci.* **11** (1976) to be published.
23. I. VOIGT-MARTIN and F. C. MULHOFF, *J. Appl. Phys.* **46** (1975) 1165.
24. G. W. LONGMAN and G. D. WIGNALL, *Polymer,* to be published.
25. G. D. WIGNALL and C.. J. PINGS, *Carbon* **12** (1974) 51.
26. R. L. MOZZI and B. E. WARREN, *J. Appl. Cryst.* **2** (1969) 164.
27. J. B. JACKSON and G. W. LONGMAN, *Polymer* **10** (1969) 873.
28. R. P. DAUBENY, C. W. BUNN and C. J. BROWN, *Proc. Roy. Soc.* **226** (1954) 531.
29. H. G. KILIAN, H. HALBOTH and E. JENCKEL, *Kolloid Z.* **172** (1960) 166.

Received 23 June 1975 and accepted 21 January 1976.